Acta Oceanol. Sin., 2018, Vol. 37, No. 9, P. 50–58
DOI: 10.1007/s13131-018-1225-1
http://www.hyxb.org.cn
E-mail: hyxbe@263.net

An evaluation of sea surface height assimilation using along-track and gridded products based on the Regional Ocean Modeling System (ROMS) and the four-dimensional variational data assimilation

ZHOU Chaojie[1, 2], DING Xiaohua[1], ZHANG Jie[2], YANG Jungang[2*], MA Qiang[1]

[1] Department of Mathematics, Harbin Institute of Technology at Weihai, Weihai 264209, China

[2] The First Institute of Oceanography, State Oceanic Administration, Qingdao 266061, China

Received 8 March 2018; accepted 27 March 2018

Abstract

Remote sensing products are significant in the data assimilation of an ocean model. Considering the resolution and space coverage of different remote sensing data, two types of sea surface height (SSH) product are employed in the assimilation, including the gridded products from AVISO and the original along-track observations used in the generation. To explore their impact on the assimilation results, an experiment focus on the South China Sea (SCS) is conducted based on the Regional Ocean Modeling System (ROMS) and the four-dimensional variational data assimilation (4DVAR) technology. The comparison with EN4 data set and Argo profile indicates that, the along-track SSH assimilation result presents to be more accurate than the gridded SSH assimilation, because some noises may have been introduced in the merging process. Moreover, the mesoscale eddy detection capability of the assimilation results is analyzed by a vector geometry–based algorithm. It is verified that, the assimilation of the gridded SSH shows superiority in describing the eddy's characteristics, since the complete structure of the ocean surface has been reconstructed by the original data merging.

Key words: ROMS, 4DVAR, sea surface height assimilation, along-track, gridded product

Citation: Zhou Chaojie, Ding Xiaohua, Zhang Jie, Yang Jungang, Ma Qiang. 2018. An evaluation of sea surface height assimilation using along-track and gridded products based on the Regional Ocean Modeling System (ROMS) and the four-dimensional variational data assimilation. Acta Oceanologica Sinica, 37(9): 50–58, doi: 10.1007/s13131-018-1225-1

1 Introduction

An efficient simulation of ocean could make a significant contribution to the prediction of oceanic dynamic progress and climate change. Using the consistency constraints with laws of time evolution and physical properties, the estimation of an ocean model state could be enhanced, when the observed information is accumulated into the oceanic model states by data assimilation technology (Bouttier and Courtier, 2002). Remote sensing has collected large mount observations with high temporal and spatial coverages, such as sea surface temperature (SST) and sea surface height (SSH). According to the research of Kurapov et al. (2011) and O'Dea et al. (2012), the accuracy of model simulation could be enhanced when the remote sensing products, such as SSH and SST, are assimilated in the model. Therefore, an excellent assimilation strategy in ocean data assimilation is becoming a meaningful issue in the oceanographic research.

Since the remote sensing observations mainly focus on the surface, the three-dimensional (3-D) ocean structure characteristics could hardly be captured directly. Cooper and Haines (1996) proposed a new algorithm to assimilate the sea surface pressure by displacing the water columns vertically. With surface pressure data assimilated every 9 d, the simulation error was reduced accordingly, but this method was designed for Cox (1985) model and cannot be applied to a free-surface model. White et al. (1990) presented an assimilation procedure of continuous altimetric sea level observations, into a realistic wind-driven numerical synoptic ocean model. The sea level observations were dynamically interpolated onto a regular grid, and then the gridded information was assimilated. Xiao et al. (2006) performed an assimilation experiment of the altimeter data based on the Princeton Ocean Model (POM), and the evaluation indicates that the accuracy of ocean currents is obviously improved. Shu et al. (2009, 2011) assimilated the SST and CTD data into a coastal model by an ensemble Kalman filter method. Benefited from the assimilation, both temperature-salinity (T-S), velocity and water mass characteristics were well simulated. Ratheesh et al. (2012) explored the usefulness of satellite-derived surface data for nowcasting of oceanic circulation features, including the SST and the sea level anomaly (SLA). Surface information was projected into the vertical using predetermined correlation functions firstly, and then both original and vertical projected observations were assimilated into the ocean model, resulted in an enhanced nowcasting capacity. Moore et al. (2011a, b, c) developed a four-dimensional variational data assimilation (4DVAR) module in the

Foundation item: The National Key Research and Development Program of China under contract No. 2016YFC1401800; the National Natural Science Foundation of China under contract Nos 41576176 and 11401140; the Key Project of Science and Technology of Harbin Institute of Technology at Weihai of China under contract No. 2014 DXGJ14.

*Corresponding author, E-mail: yangjg@fio.org.cn

ROMS. In the 4DVAR, all the available observations over a finite time interval were taken into consideration, in order to identify the global optimal estimation of ocean states.

The assimilation would be benefited when the SSH is introduced into the ocean model efficiently. Regularly, the altimeter missions sample the sea level along their ground tracks every 7 km, result in the limited coverage of the along-track SSH data. Considering the continuous variation characteristics of the sea level (Gill, 1982), a gridded SSH product named Archiving Validation and Interpretation of Satellite Oceanographic (AVISO) is generated by merging the multi satellite altimeter data. Compared with the along-track observations, the complete structure of the ocean surface is reconstructed.

In this paper, we will analyze the impact of the two SSH data sets on the assimilation, based on the ROMS and an incremental strong constraint 4DVAR method. First, the model configuration, the twin experiment and the validation data are introduced in Section 2; Section 3 is the main body, both the accuracy and the eddy detection capability of the experiment results are discussed. In Section 3.1, the accuracy analysis is conducted with the EN4 data set and Argo (array for real-time geostrophic oceanography) T-S profiles, while the evaluation of eddy detection capability is presented in Section 3.2. At last, some final remarks are given in Section 4.

2 Experiment configuration and data

2.1 *Model configuration*

The ROMS is a free-surface, hydrostatic, primitive equation model discretized with a terrain following vertical coordinate system (Shchepetkin and McWilliams, 2005). The model domain covers the whole South China Sea (SCS) and its adjacent area from 1° to 30°N, 99° to 134°E (Fig. 1), with an eddy-resolved horizontal resolution of 0.1°×0.1° (about 10 km) and 30 S-coordinate layers in the vertical. The level 2.5 Mellor Yamada (1982) scheme is adopted as the parameterization of the vertical mixing process. The temperature and salinity fields are initialized by the Levitus climatology data set, while the free surface and velocity are set as 0. The ETOPO1 data (Amante and Eakins, 2009) is employed to produce the bathymetry field, and the minimum and maximum depths in the whole domain are set to be 10 and 5 000 m, respectively. The wind field employs a daily mean wind field from the Cross-Calibrated Multi-Platform (CCMP) ocean surface wind product (Atlas et al., 2011) with a horizontal resolution of 0.25°×0.25°, which is converted into the wind stress using the bulk formula given by Large and Pond (1982). The other daily atmospheric forcing fields, including heat fluxes, solar radiation fluxes, evaporation-precipitation (E-P), air temperature and specific humidity, are obtained from the National Centers of Environmental Prediction (NCEP) reanalysis with a horizontal resolution of 1.875°×1.875° (Kalnay et al., 1996). Finally, the lateral boundary conditions, including the monthly temperature, salinity, sea surface height and velocity field are provided by the Simple Ocean Data Assimilation (SODA) data set.

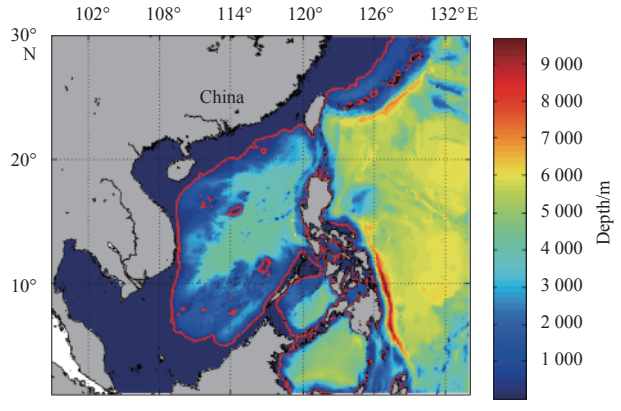

Fig. 1. Model domain and bathymetry. The red contour represents the 200 m isobath.

2.2 *Assimilation configuration*

The model comes to an ocean dynamic balanced state after 5 a integration starts from January 1, 2002. Then the SSH assimilation experiment is conducted during January 2007. In the data assimilation progress, the forcing and the boundary fields remain the same as prior model simulation. Advanced Very High-Resolution Radiometer (AVHRR) SST provided by the NOAA is employed for its high quality. It is a gridded product with a resolution of 0.25°×0.25° and is produced by merging the satellite observations and *in situ* measurements based on the optimal interpolation (Reynolds et al., 2007). To facilitate the calculation, the AVHRR is reduced to 1°×1° by selecting every four grids.

The SSH used in the experiment is provided by the AVISO, with the support from the Centre National D'études Spatiales (CNES). The gridded product is available every day since July 2006, and the spatial resolution is 0.25°×0.25°. The corresponding along-track SSH observations merged in the gridded products are also available. In the experiment, the original along-track observations and the gridded product from the AVISO are assimilated to evaluate their impact on the assimilation. To ensure the comparability, we use the original along-track observations of the gridded product merging in the assimilation, and the SSH derived from Jason-1, GFO and Envisat is gathered for the twin experiment. Since the reference level of the SSH and ROMS free surface is different, the steric signal is removed firstly using the result of Willis et al. (2004). The AVISO sea surface height anomalies (SSHA) with the steric signal removed is then added to the mean model height (Fig. 2). Compared with the processed AVISO "SSH", the main spatial characteristics have been captured by the prior model simulation. According to the study of Powell et al. (2008) focus on the assimilation interval, a 7 d assimilation interval on the model solutions is chosen in this paper.

The goal of 4DVAR is to identify the best estimate circulation (commonly referred to as the analysis or posterior), by minimizing the difference between the model and the observations in a least-squares sense, with a prior hypothesis about errors and possibly additional constraints. Moreover, the errors and uncertainties of initial conditions, surface forcing, and boundary conditions are all taken into consideration in the cost function. Therefore, the three fields are referred to as control variables, and the problem in the 4DVAR is reduced to identifying the appropriate combination of control variables that yield the best estimation over a finite time interval.

The choice of parameters for modeling the background error covariance matrix ($\boldsymbol{D}$) and the observation error covariance matrix ($\boldsymbol{R}$) are designed as Moore et al. (2011b). The background errors of all initial condition control variable components of the background error covariance matrix are considered to be correlative for 50 km in the horizontal and 30 m in the vertical. Horizontal correlation scales chosen for the background surface forcing error components of the background error covariance matrix are 300 km for wind stress and 100 km for heat and freshwater fluxes. The correlation lengths for the background open bound-

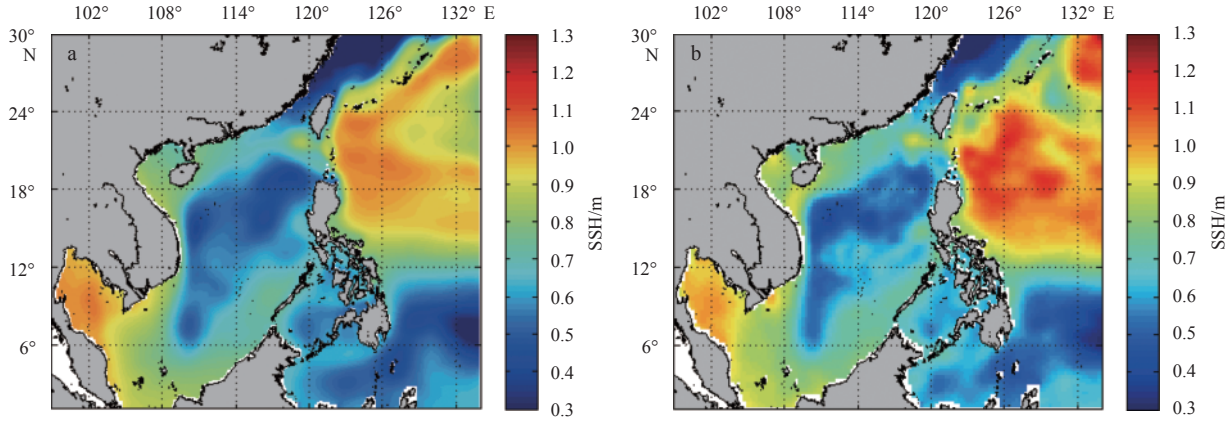

Fig. 2. Model SSH (a) and processed AVISO SSH (b) (with the steric signal removed and the mean model height added).

ary condition error components of the background error covariance matrix are chosen to be 100 km in the horizontal and 30 m in the vertical. Observation errors are assumed to be uncorrelated in space and time, and the variances along the main diagonal of the observation error covariance matrix are assigned as a combination of measurement error and the error of representativeness. The measurement errors of the AVISO SSHA and the AVHRR SST are chosen as the following standard deviations: 0.02 m for the SSHA, 0.4°C for the SST.

In order to explore the impact of the two SSH data on the assimilation, four cases are designed as Table 1. The 1°×1° reduced SST is assimilated in both the four cases. Case 1 is designed as the control experiment and no SSH is assimilated, while the reduced gridded SSH of 1°×1° is assimilated in Case 2, the gridded SSH with an original resolution (0.25°×0.25°) is considered in Case 3 and the along-track SSH observations are employed in Case 4. Here Case 2 is designed to make the strength of gridded products clearer.

Table 1. Resolution of data assimilated in Cases 1–4

	Case 1	Case 2	Case 3	Case 4
SST/°C	1°×1°	1°×1°	1°×1°	1°×1°
SLA/m	none	1°×1°	0.25°×0.25°	along-track

2.3 *Validation data*

To evaluate the accuracy of the experiment results, the EN4 data set and Argo T-S profiles are employed as the validation data. The EN4 gridded data set is a global monthly objective analyzed ocean T-S product, generated by Hadley Centre of the UK Met Office. It covers the period from 1900 to present. Observations from all types of ocean profiling instruments with T-S information are ingested into the data set (Good et al., 2013). The spatial resolution is 1°×1° in the horizontal and 42 layers in the vertical.

The Argo project is designed to observe large-scale subsurface ocean T-S profiles globally. The observation starts from the surface and may reach 2 000 m depth, with a complete cycle of 10 d (Roemmich and Gilson, 2009). In this paper, the Argo temperature profiles are obtained from the China Argo Real-Time Data Center and the Global Data Assembly Centre (Argo, 2000). After temporal-spatial matching and quality control, 35 profiles are left and the distribution is shown in Fig. 3.

3 Results

The gridded SSH products are supposed to hold the complete reconstructed structure on the surface, but the resolution

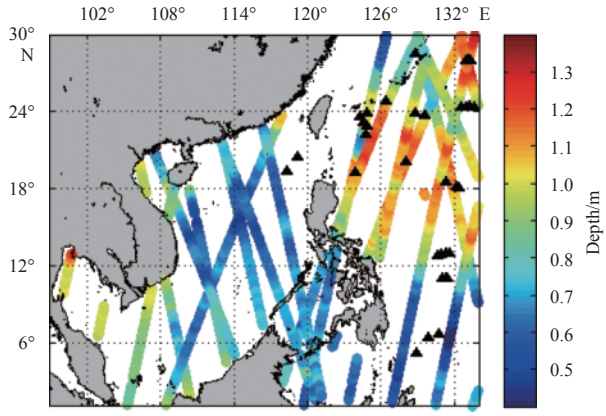

Fig. 3. Location of the matched Argo profiles (blue triangle) during January 2007, the orbit represents the along-track SSH observations (AVISO) added the mean model height.

(0.25°×0.25°) is lower than the original observations (7 km) along the orbit of altimetry. Owning to the different strength of the two SSH data, the assimilation results would present different properties accordingly. In this section, both the accuracy and eddy detection capability of the outcomes would be discussed.

3.1 *Accuracy analysis*

To analyze the accuracy of the experiment globally, the results of the cases are compared with the EN4 data. First, monthly average of the result is calculated, and then interpolated to 3-D grid of EN4 from the vertical and horizontal, respectively. A horizontal absolute bias (HAB, $b_{\mathrm{a,h}}$) and vertical absolute bias (VAB, $b_{\mathrm{a,v}}$) above 5 000 m are calculated as follows:

$$b_{\mathrm{a,h}} = \frac{1}{N_1}\sum_{k=1}^{N_1}\left|M\left(i,j,k\right) - E\left(i,j,k\right)\right|, \tag{1}$$

$$b_{\mathrm{a,v}} = \frac{1}{N_2 N_3}\sum_{j=1}^{N_2}\sum_{i=1}^{N_3}\left|M\left(i,j,k\right) - E\left(i,j,k\right)\right|, \tag{2}$$

where M and E represent the assimilation result and EN4 data; N_1 is the total vertical layers of EN4 above 5 000 m; N_2 and N_3 stand for the horizontal dimensions of EN4.

As shown in Fig. 4, Cases 2–4 with the SSH assimilation both

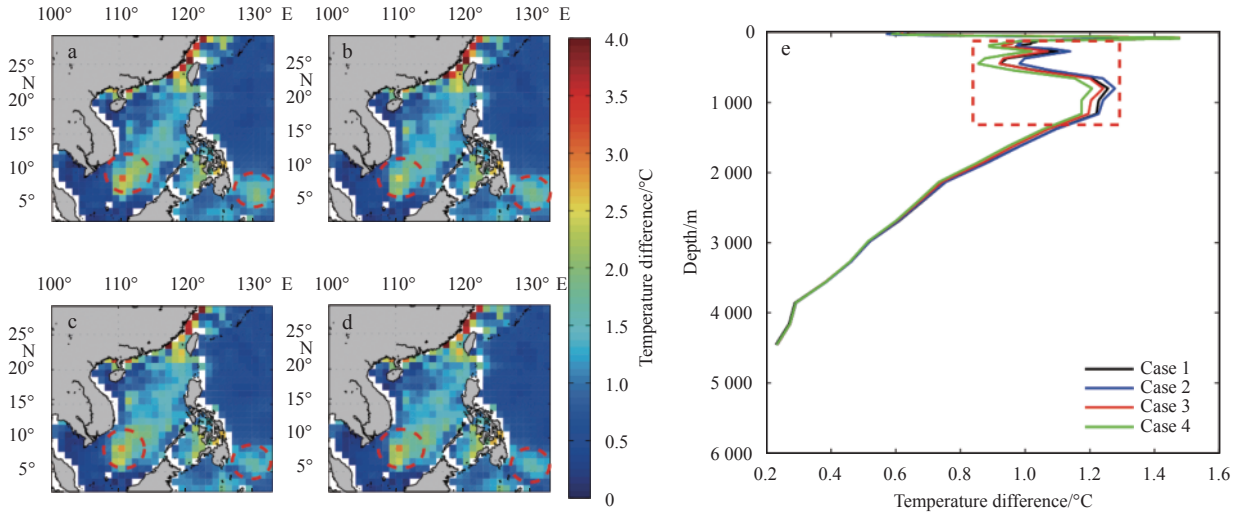

Fig. 4. HAB (a, c) and VAB (b, d) distribution of four cases above 5 000 m depth. a–d. The horizontal error distribution of Cases 1–4; and e. the vertical error distribution.

achieve a promotion in the vertical and horizontal. Respectively, the HAB of ocean temperature of the southern SCS and the northeastern Taiwan obtains a remarkable enhancement, and may reach up to 2°C; the VAB distribution in Fig. 4b indicates that, the absolute bias would also decrease after the SSH assimilation. Case 4 with along-track observations assimilated obtains the best performance, followed by Case 3. The VAB mainly occurs in the 200–1 200 m and the absolute bias could exceed 1°C. In order to present the impact of different SSH products expressly, the global averaged absolute bias between the four cases and EN4 are collected. As shown in Table 2, Case 4 seizes the smallest temperature (0.87°C) and salinity (0.076) error, while the gridded SSH assimilation cases get the medium ones.

In the following section, the Argo profile is applied to validate the accuracy of the four cases locally. Considering the micro enhancement of salinity in the assimilation experiment, we mainly concentrate our attention on the comparison of temperature. The outcomes of the assimilation are interpolated to the measure position of each Argo profile sequentially, first in the vertical and then in the horizontal. Ultimately, 2 113 matched temperature measurements of Argo are obtained. To evaluate the results' accuracy, both an absolute bias (A-Bias) and a root mean square error (RMSE) are calculated. As shown in Fig. 5, Cases 2–4 have an accuracy promotion after the SSH assimilation, no matter which SSH data were ingested. Generally, the difference mostly occurs in 10–25°C and the model outcome seems to be the higher one. Moreover, the Case 3 with original gridded SSH assimilated seizes the best accuracy (A-Bias: 0.77°C, RMSE: 1.14°C), which is contrary to the comparison with EN4. Here, the unbalanced distribution of the Argo profiles ought to be punished, because more Argo profiles are located beyond the altimetry track, making the conclusion one-sided.

Furthermore, compared with the location of altimeter track, the temporal matched Argo profiles are divided into two parts: along the track or beyond the track. The spatial interval 25 km of the gridded SSH product is chosen as the threshold value, and 11 along-track and 24 beyond-track profiles are obtained, respectively. The representative classification of Argo profiles of 2007-01-01 and 2007-01-26 is presented in Fig. 6. The accuracy analysis of the two separated profile groups is illustrated in Fig. 7, and the A-Bias and the RMSE are appended as well. Compared with Case 1, Case 4 performs the best with a reduction of 0.154°C (RMSE) and 0.08°C (A-Bias) along the altimeter track. Accordingly, Case 3 holds an enhancement of 0.147°C and 0.05°C. Beyond the altimeter track, similar promotion of accuracy can hardly be obtained in Case 4, due to the limited influence of the along-track observations. However, there still exists some slight promotion, by the benefit of the global optimization capacity of the 4DVAR.

Table 2. Averaged difference of T-S between EN4 and Cases 1–4

	Case 1	Case 2	Case 3	Case 4
Temperature/°C	0.900 1	0.898 0	0.891 7	0.871 3
Salinity	0.077 6	0.077 4	0.076 6	0.075 7

3.2 *Eddy detection capability*

According to the research of Zhang et al. (2014), a mesoscale eddy plays an important role in the oceanic transports of heat, salt, fresh water, dissolved CO_2, and other tracers. Therefore, an accurate simulation of eddy is necessary in the research of ocean dynamics. In our experiment, the model is configured with an eddy-resolved horizontal resolution 0.1°×0.1°, and is enough to capture the main structure of eddy. In this section, the vector geometry–based eddy detection algorithm (Nencioli et al., 2010) method is employed, to evaluate the eddy detection capability of the four assimilation cases.

As presented in Fig. 8, Case 1 without the SSH assimilation has already gained the ability in eddy capture, and the eddies derived from the Kuroshio Current could be well characterized. Moreover, the detection of eddy are strengthened after the SSH assimilation. To acquire a quantitative analysis, we calculate the radius and eddy kinetic energy (EKE, $E_{k,e}$) of the detected eddies during January 2007. The specific algorithm (Penven et al., 2005) is given as follows:

$$R = \sqrt{\frac{A}{\pi}}\,, \tag{3}$$

$$E_{k,e} = \frac{1}{2N}\sum_{i=1}^{N}(u'^{2}_{i} + v'^{2}_{i})\,, \tag{4}$$

where A represents the area of the eddy; R is the radius of a

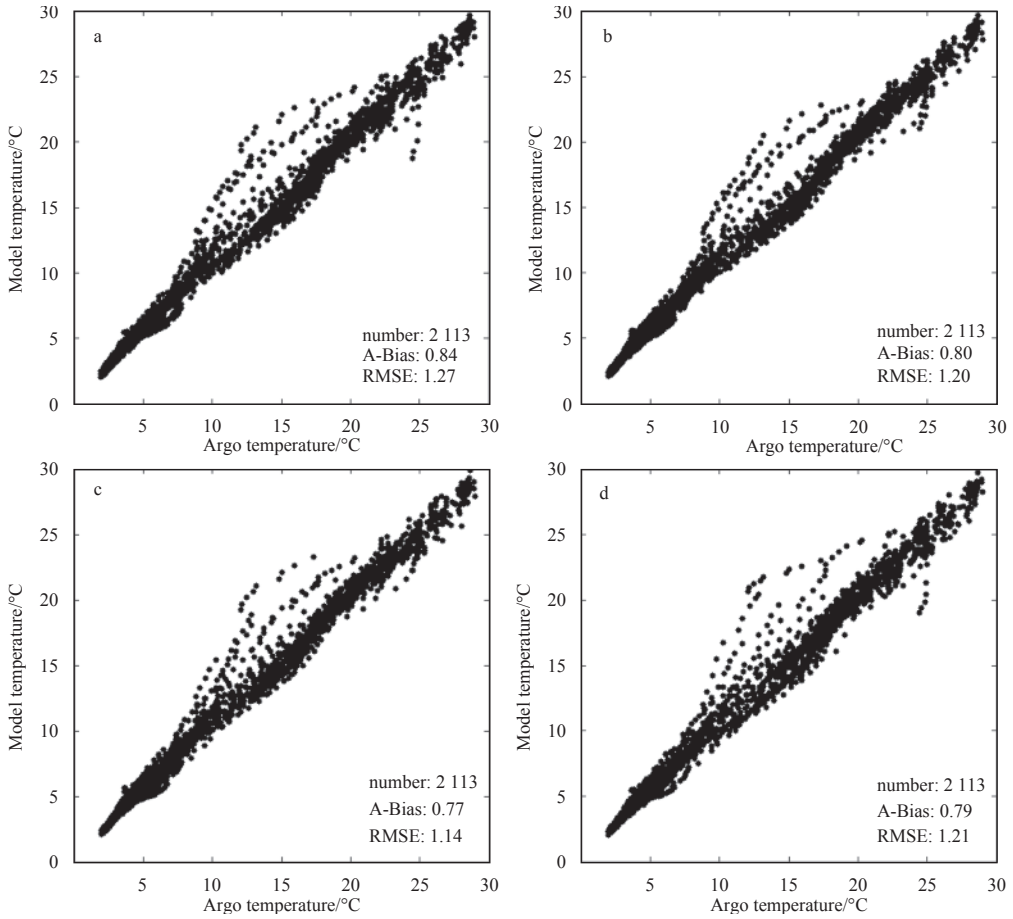

Fig. 5. Scatter diagrams of assimilation results versus Argo profiles. a–d represent the comparison results of Cases 1–4, respectively.

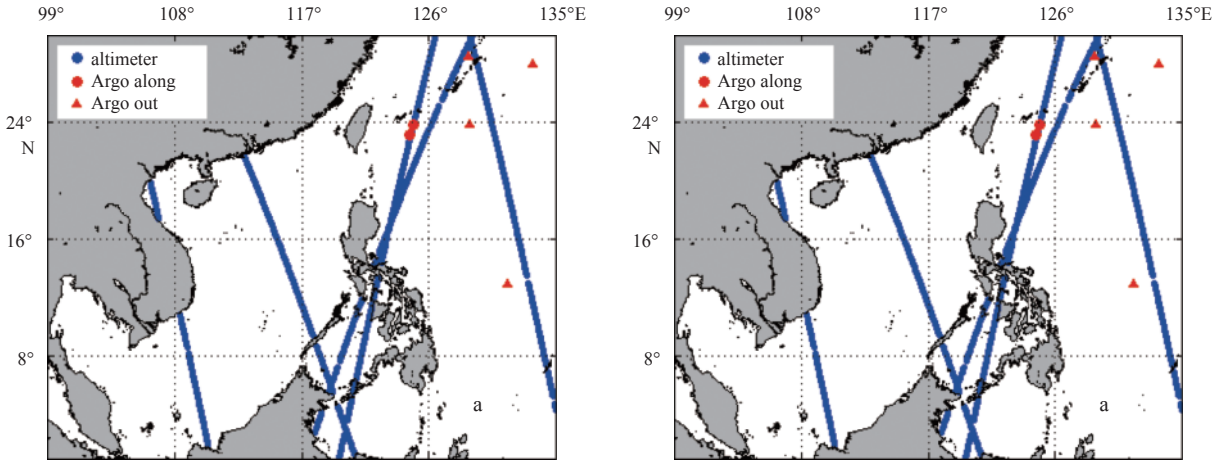

Fig. 6. Classification of Argo profiles on 2007-01-01 (a) and 2007-01-26 (b).

circle with the same area A; N means the total number of grids involved in an eddy; and u'_i and v'_i are the horizontal velocity anomaly of grid i, here $i = 1, 2, \cdots, N$.

The distribution of radius and EKE of detected eddies are shown in Fig. 9. We can see that, the radius and EKE of the detected eddies are smaller than 150 km and 1 500 cm^2/s^2, which meets the conclusion of Cheng and Qi (2010) well. Besides, the number, radius and EKE of detected eddies are presented in Table 3. The total number of detected eddies increases significantly after the SSH assimilation. However, both the averaged radius and EKE of Cases 2 and 4 are tending to decay, because of the low resolution and bad coverage of the SSH. After all, the capability of Case 4 seems to be the most remarkable one in ocean mesoscale eddy detection, as the complete structure characteristics of eddy have been reconstructed by the merging procedure.

4 Conclusions

In order to explore the impact of the SSH types (along-track and gridded) on the data assimilation, a twin experiment with four cases is conducted based on the ROMS and the 4DVAR. In the accuracy analysis, the EN4 data set and the Argo profiles are employed to validate the assimilation results globally and locally. The comparison with EN4 indicates that, Case 4 with the along-track SSH assimilation seizes the best accuracy. Though the gridded SSH is equipped with the better coverage, the "valid" observations are limited because the 0.25°×0.25° resolution is lower than the density of altimeter original measurements (7 km). Difference occurs in the comparison with the Argo profiles. The averaged error of the gridded SSH assimilation in Case 3 presents an optimal accuracy, where the centralized distribution of validation profiles in the analysis should be punished. Then the validation profiles are divided into two groups: along-track and beyond-track, by considering their distance with the nearest altimeter observations. Case 4 with the along-track SSH assimilation presents a higher accuracy promotion along the track, while slight error reduction beyond the track.

Besides, the mesoscale eddy detection capability of the model result is discussed. In this paper, the statistical characteristics

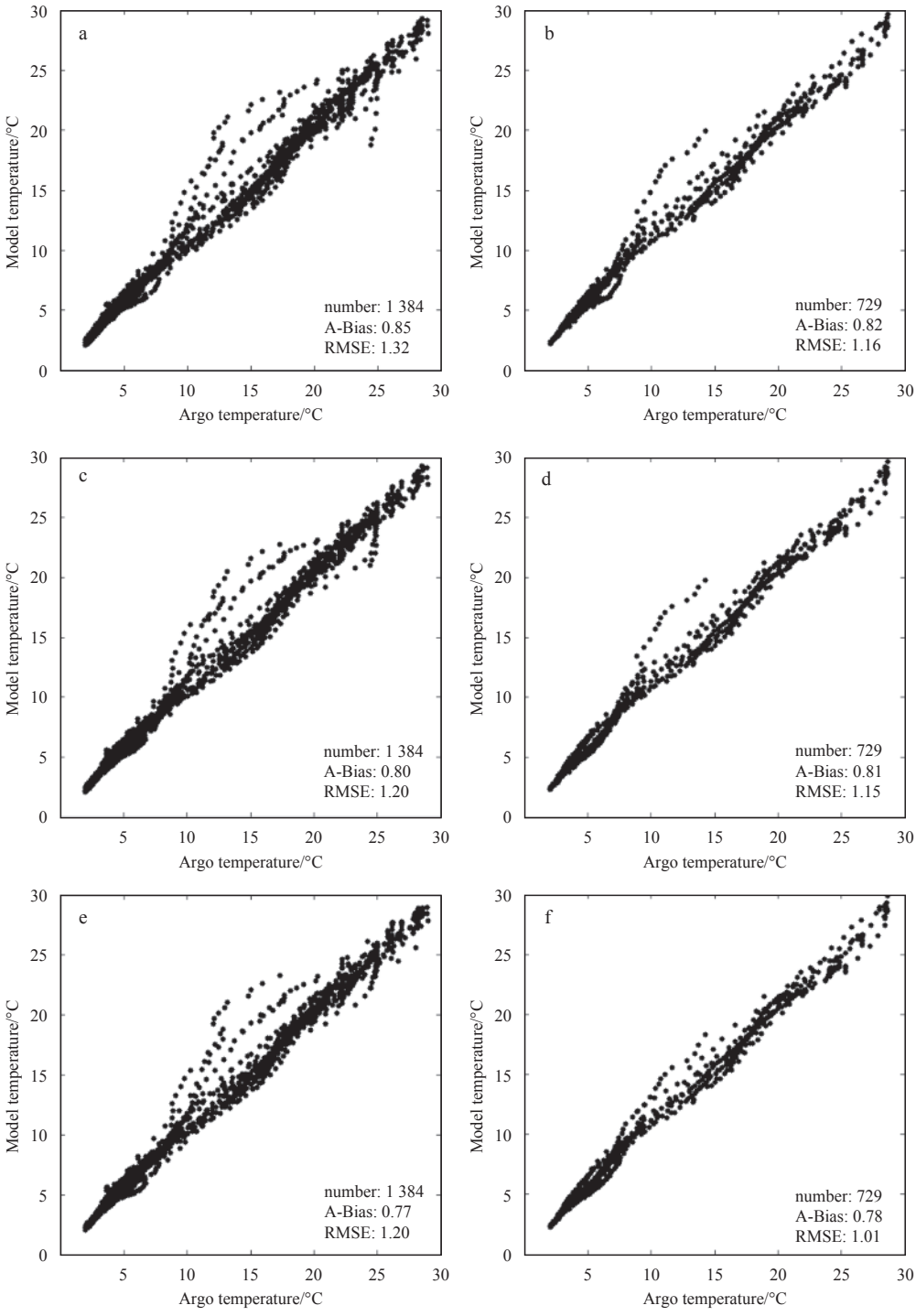

Fig. 7.

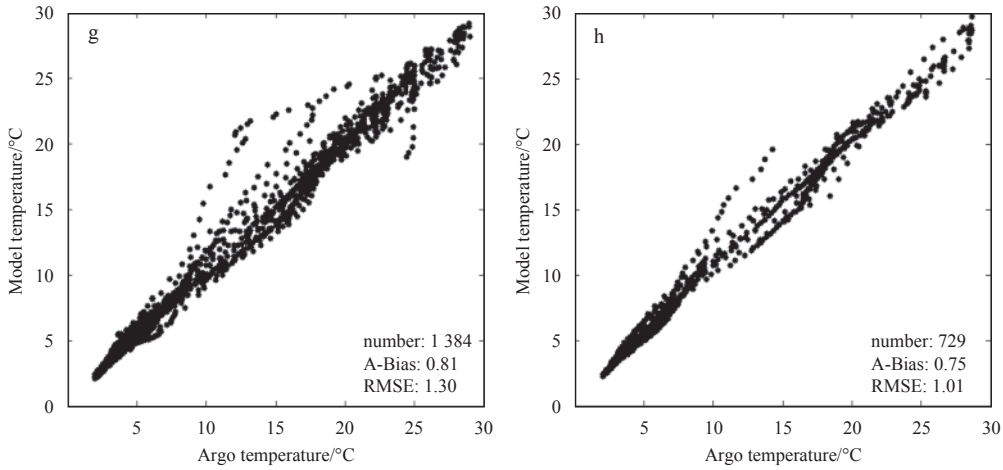

Fig. 7. Scatter diagrams of assimilation results versus the beyond-track (a, c, e and g) and the along-track (b, d, f and h) Argo profiles of Cases 1–4 (a–h).

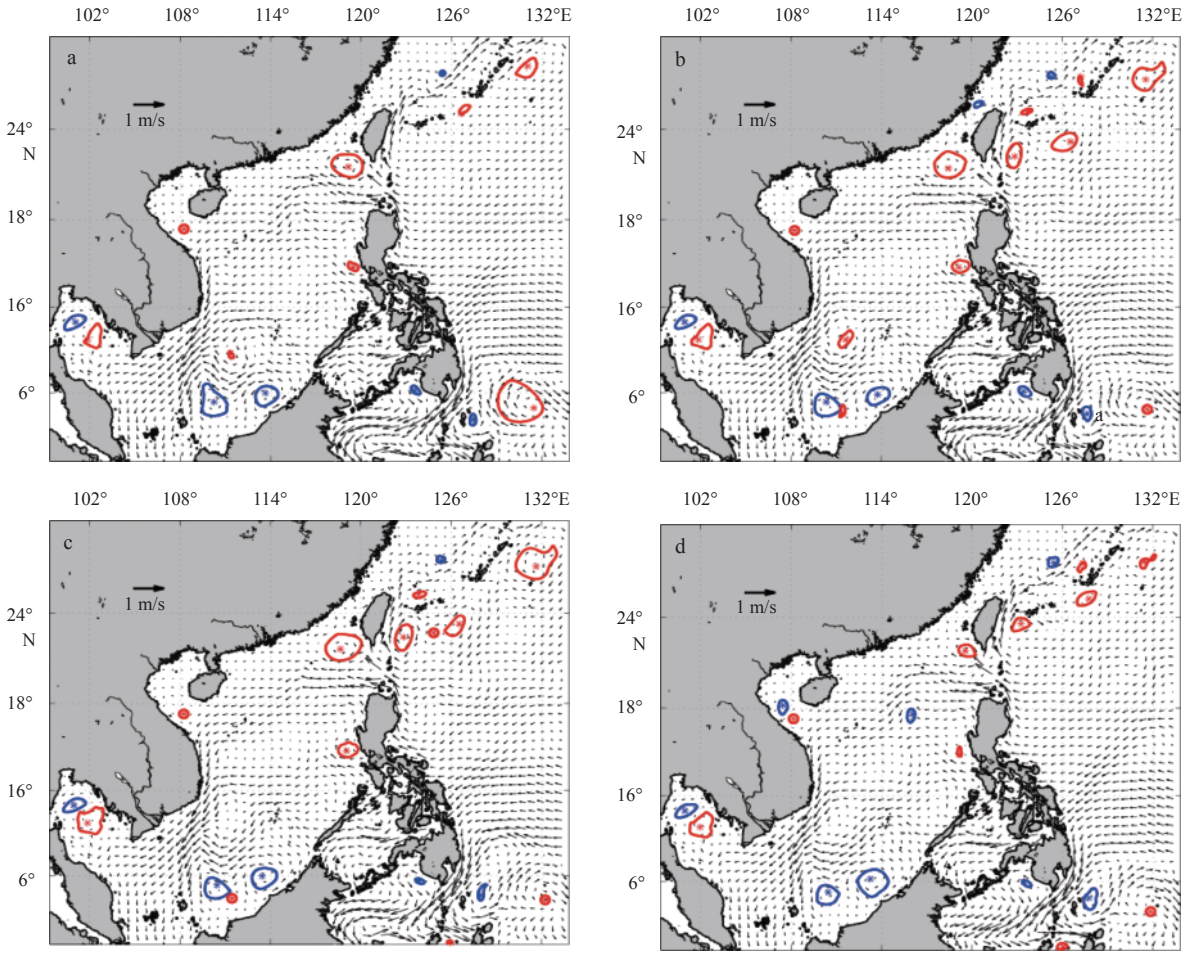

Fig. 8. Detected eddies and currents on 2007-01-31. a–d represent the results of Cases 1–4, respectively.

of the detected eddies, including the number, the radius and the EKE is studied. Because the complete ocean structure is reconstructed in the gridded SSH products, more reasonable eddies are detected out in Case 3. Totally speaking, both the along-track and gridded SSH products have a significant effect on the data assimilation. The along-track SSH product has more real observations, while the gridded one contains more complete characteristics. When assimilated into the ROMS, higher accuracy can be achieved by the benefit of real observations with the along-track observations, and more reasonable ocean mesoscale eddy char-

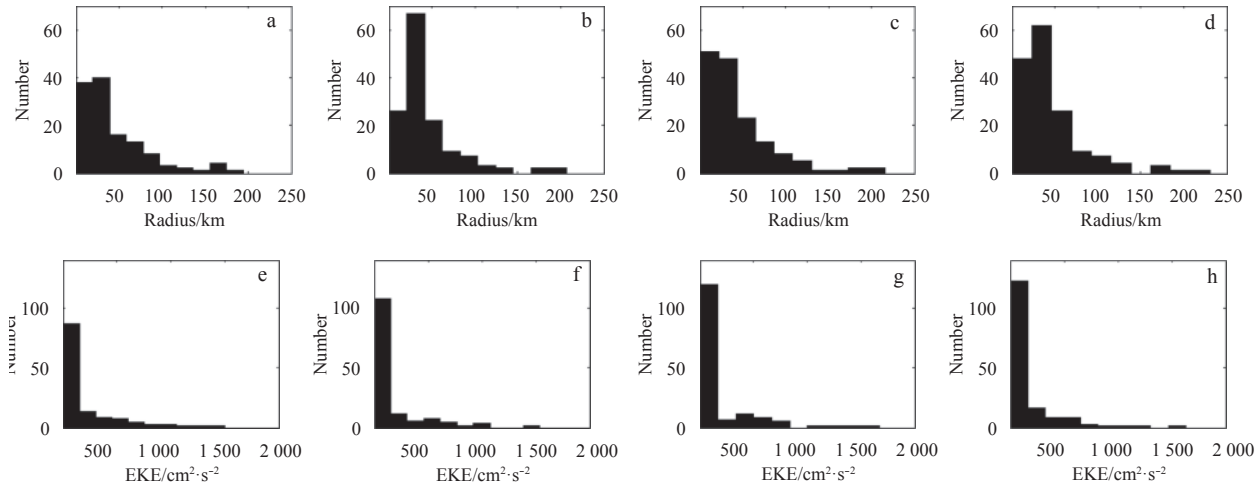

Fig. 9. Distributions of radius (a–d) and EKE (e–h) of the detected eddies during January 2007. a–d and e–h are the statistical results of Cases 1–4, respectively.

Table 3. Statistical characteristics of the detected eddies in Cases 1–4

	Case 1	Case 2	Case 3	Case 4
Cyclonic	47	56	50	54
Anticyclonic	46	65	59	65
Mean radius/km	56.0	49.4	57.5	54.8
EKE/cm^2·s^{-2}	244.5	165.4	210.7	182.8

acteristics can be detected with the gridded product.

References

Amante C, Eakins B W. ETOPO1 1 Arc-Minute Global Relief Model: Procedures, Data Sources and Analysis. Psychologist 2009. ETOPO1 1 Arc-Minute Global Relief Model: Procedures, Data Sources and Analysis. Psychologist, 16(3): 20–25

Argo. 2000. Argo float data and metadata from Global Data Assembly Centre (Argo GDAC). SEANOE. http://doi.org/10.17882/42182 [2000-09-12/2015-9-20]

Atlas R, Hoffman R N, Ardizzone J, et al. 2011. A cross-calibrated, multiplatform ocean surface wind velocity product for meteorological and oceanographic applications. Bulletin of the American Meteorological Society, 92(2): 157–174

Bouttier F, Courtier P. 1999. Data assimilation concepts and methods March 1999. Bracknell: ECMWF, 59

Cheng Xuhua, Qi Yiquan. 2010. Variations of eddy kinetic energy in the South China Sea. Journal of Oceanography, 66(1): 85–94

Cooper M, Haines K. 1996. Altimetric assimilation with water property conservation. Journal of Geophysical Research, 101(C1): 1059–1077

Cox M D. 1985. An eddy resolving numerical model of the ventilated thermocline. Journal of Physical Oceanography, 15(10): 1312–1324

Gill A E. 1982. Atmosphere-Ocean Dynamics. London: Academic Press, 345–346

Good S A, Martin M J, Rayner N A. 2013. EN4: quality controlled ocean temperature and salinity profiles and monthly objective analyses with uncertainty estimates. Journal of Geophysical Research: Oceans, 118(12): 6704–6716

Kalnay E, Kanamitsu M, Kistler R, et al. 1996. The NCEP/NCAR 40-year reanalysis project. Bulletin of the American Meteorological Society, 77(3): 437–471

Kurapov A L, Foley D, Strub P T, et al. 2011. Variational assimilation of satellite observations in a coastal ocean model off Oregon. Journal of Geophysical Research: Oceans, 116(C5): C05006

Large W G, Pond S. 1982. Sensible and latent heat flux measurements over the ocean. Journal of Physical Oceanography, 12(5): 464–482

Mellor G L, Yamada T. 1982. Development of a turbulence closure model for geophysical fluid problems. Reviews of Geophysics, 20(4): 851–875

Moore A M, Arango H G, Broquet G, et al. 2011a. The Regional Ocean Modeling System (ROMS) 4-dimensional variational data assimilation systems: Part I—System overview and formulation. Progress in Oceanography, 91(1): 34–49

Moore A M, Arango H G, Broquet G, et al. 2011b. The Regional Ocean Modeling System (ROMS) 4-dimensional variational data assimilation systems: Part II—Performance and application to the California Current System. Progress in Oceanography, 91(1): 50–73

Moore A M, Arango H G, Broquet G, et al. 2011c. The Regional Ocean Modeling System (ROMS) 4-dimensional variational data assimilation systems: Part III—Observation impact and observation sensitivity in the California Current System. Progress in Oceanography, 91(1): 74–94

Nencioli F, Dong Changming, Dickey T, et al. 2010. A vector geometry-based eddy detection algorithm and its application to a high-resolution numerical model product and high-frequency radar surface velocities in the Southern California Bight. Journal of Atmospheric and Oceanic Technology, 27(3): 564–579

O'Dea E J, Arnold A K, Edwards K P, et al. 2012. An operational ocean forecast system incorporating NEMO and SST data assimilation for the tidally driven European North-West shelf. Journal of Operational Oceanography, 5(1): 3–17

Penven P, Echevin V, Pasapera J, et al. 2005. Average circulation, seasonal cycle, and mesoscale dynamics of the Peru Current System: A modeling approach. Journal of Geophysical Research: Atmospheres, 110(C10): C10021

Powell B S, Arango H G, Moore A M, et al. 2008. 4DVAR data assimilation in the Intra-Americas Sea with the Regional Ocean Modeling System (ROMS). Ocean Modelling, 23(3–4): 130–145

Ratheesh S, Sharma R, Basu S. 2012. Projection-based assimilation of satellite-derived surface data in an Indian Ocean circulation model. Marine Geodesy, 35(2): 175–187

Reynolds R W, Smith T M, Liu Chunying, et al. 2007. Daily high-resolution-blended analyses for sea surface temperature. Journal of Climate, 20(22): 5473–5496

Roemmich D, Gilson J. 2009. The 2004–2008 mean and annual cycle of temperature, salinity, and steric height in the global ocean from the Argo program. Progress in Oceanography, 82(2): 81–100

Shchepetkin A F, McWilliams J C. 2005. The Regional Oceanic Modeling System (ROMS): A split-explicit, free-surface, topography-

following coordinates oceanic model. Ocean Modelling, 9(4): 347–404

Shu Yeqiang, Zhu Jiang, Wang Dongxiao, et al. 2009. Performance of four sea surface temperature assimilation schemes in the South China Sea. Continental Shelf Research, 29(11–12): 1489–1501

Shu Yeqiang, Zhu Jiang, Wang Dongxiao, et al. 2011. Assimilating remote sensing and in situ observations into a coastal model of northern South China Sea using ensemble Kalman filter. Continental Shelf Research, 31(6): S24–S36

White W B, Tai C K, Holland W R. 1990. Continuous assimilation of Geosat altimetric sea level observations into a numerical synoptic ocean model of the California Current. Journal of Geophysical Research: Oceans, 95(C3): 3127–3148

Willis J K, Roemmich D, Cornuelle B. 2004. Interannual variability in upper ocean heat content, temperature, and thermosteric expansion on global scales. Journal of Geophysical Research: Oceans, 109(C12): C12036

Xiao Xianjun, Wang Dongxiao, Xu Jianjun. 2006. The assimilation experiment in the southwestern South China Sea in summer 2000. Chinese Science Bulletin, 51(S2): 31–37

Zhang Zhengguang, Wang Wei, Qiu Bo. 2014. Oceanic mass transport by mesoscale eddies. Science, 345(6194): 322–324